Organic Electronics 13 (2012) 147–152

Contents lists available at SciVerse ScienceDirect

Organic Electronics

journal homepage: www.elsevier.com/locate/orgel

The operational mechanism of ferroelectric-driven organic resistive switches

Martijn Kemerink [a,*], Kamal Asadi [b,d], Paul W.M. Blom [b,c], Dago M. de Leeuw [b,d]

[a] Department of Applied Physics, Eindhoven University of Technology, P.O. Box 513, 5600 MB Eindhoven, The Netherlands
[b] Zernike Institute for Advanced Materials, University of Groningen, Nijenborgh 4, 9747 AG Groningen, The Netherlands
[c] Holst Centre, High Tech Campus 31, 5605 KN Eindhoven, The Netherlands
[d] Philips Research Laboratories, High Tech Campus 4, 5656 AE Eindhoven, The Netherlands

ARTICLE INFO

Article history:
Received 17 October 2011
Accepted 20 October 2011
Available online 7 November 2011

Keywords:
Charge transport
Organic semiconductors
Ferroelectric nanostructures
Data storage
Thin films

ABSTRACT

The availability of a reliable memory element is crucial for the fabrication of 'plastic' logic circuits. We use numerical simulations to show that the switching mechanism of ferroelectric-driven organic resistive switches is the stray field of the polarized ferroelectric phase. The stray field modulates the charge injection from a metallic electrode into the organic semiconductor, switching the diode from injection limited to space charge limited. The modeling rationalizes the previously observed exponential dependence of the on/off ratio on injection barrier height. We find a lower limit of about 50 nm for the feature size that can be used in a crossbar array, translating into a rewritable memory with an information density of the order of 1 Gb/cm^2.

The availability of a reliable memory element is crucial for the fabrication of 'plastic' logic circuits [1]. A number of strategies for making organic resistive switches has been proposed and implemented [2]. These can be separated into write-once and rewritable, write-many-times memories. Working examples of the former type have been based on fuses [3,4] and might find use in low cost, disposable devices, such as programmable RFID-tags [5]. For applications in which erase and rewrite functionality is required this concept cannot be used. One of the promising routes to a fully organic rewritable memory element is to split the switching functionality from the read-out operation [6]. This approach is typical for memories based on the electrically insulating ferroelectric polymer, poly(vinylidenefluoride-co-trifluorethylene) (P(VDF-TrFE)), [7] where the ferroelectric P(VDF-TrFE) provides the switching functionality and the read-out operation is performed by conduction through a nearby semiconducting layer [8,9].

Resistive switching and non-destructive read-out has been demonstrated in both transistors [8] and diodes [9]. The operation of ferroelectric field-effect transistors is relatively straightforward. The polarization of the ferroelectric gate insulator does (On) or does not (Off) induce an accumulation layer in the semiconducting channel [10]. The operation of the bistable diodes, realized by blending the ferroelectric P(VDF-TrFE) with a semiconductor, is based on the modulation of the injection barrier. It was suggested that in the case of a *p*-type semiconductor, negative ferroelectric polarization at the injecting contact is compensated by accumulated holes in the semiconductor. The resulting band bending then effectively lowers the injection barrier and, hence, the resistance of the diode. Excellent current rectification and high on/off current ratios have been reported for this type of device [11].

To explain the hole accumulation and band bending, a particular 3D morphology was initially adopted in which the ferroelectric phase has an undercut at the injecting electrode, which is filled with the semiconductor, as schematically shown in Fig. 1a [9,11]. However, thorough morphological analysis has shown that upon spincoating the

* Corresponding author.
E-mail address: m.kemerink@tue.nl (M. Kemerink).

1566-1199/$ - see front matter © 2011 Elsevier B.V. All rights reserved.
doi:10.1016/j.orgel.2011.10.013

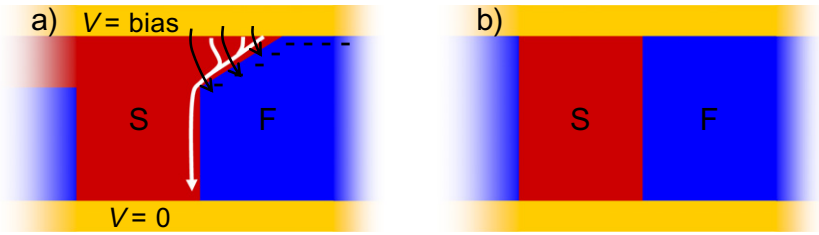

Fig. 1. (a) Previously proposed morphology and operation for ferroelectric-driven organic resistive switches with undercut in the ferroelectric phase (F), filled with semiconductor (S). Black and white arrows indicate electric fields and current flow, respectively. Minuses (−) indicate polarization charges in the ferroelectric. (b) Simplified morphology used in the numerical calculations. (For interpretation of the references to color in this figure legend, the reader is referred to the web version of this article.)

blend phase-separates into semiconductor-rich domains embedded in a crystalline P(VDF-TrFE) matrix [12]. Synchrotron-based scanning transmission X-ray microscopy and atomic force microscopy measurements have shown that the semiconductor domains are columnar and bicontinuous throughout the film, as schematically depicted in Fig. 1b [13]. The presence of columnar semiconducting domains rules out the initially proposed morphology of Fig. 1a. In order to design memories based on phase separated ferroelectric/semiconductor blends, the vital question is therefore to understand the true origin of the switching and of the modulation of the injection barrier. To address this question, here we adopt a simplified morphological model in which the edges of the two phases are straight and perpendicular to the electrode surface (Fig. 1b). We show by numerical simulation of a diode with this simplified morphology that the switching between an injection-limited Off-state and a space charge limited On-state is reproduced. *We demonstrate that the driving force for resistance switching of the diode is the stray field of the polarized ferroelectric phase.* Furthermore, we quantitatively reproduce the experimentally observed exponential scaling of the on/off current modulation ratio with injection barrier height. Finally, we estimate the optimum diameter of the semiconducting domains in a ferroelectric matrix and hereby predict the ultimate memory density that can be realized.

The electrical transport model is based on the coupled drift–diffusion, Poisson, and current continuity equations that are numerically solved on a rectangular grid [14]. The 3D phase separated morphology is therefore mapped onto a simplified 2D structure of alternating ferroelectric and semiconducting slabs, implemented by periodic boundary conditions, as shown in Fig. 2a. The electric current runs only through the semiconducting phase since the ferroelectric P(VDF-TrFE) is an insulator. The ferroelectric slab is therefore characterized by a zero mobility and a large (>1 eV) HOMO offset with respect to the semiconductor. In the ferroelectric slab a surface polarization charge density $\sigma_p \sim 70\ \mathrm{mC/m^2}$ can be fixed on the first grid points, 1.5 nm above the bottom electrode and below the top electrode. A static relative dielectric constant of $\varepsilon_r = 10$ was used. The organic semiconducting slab was characterized by a typical constant hole mobility, μ_p, of $6.5 \times 10^{-11}\ \mathrm{m^2/Vs}$ and $\varepsilon_r = 2.5$. Use of a charge density-dependent hole mobility gave qualitatively identical results. The hole injection barrier at the top contact, φ_t, was varied between 0.1 and 1.1 eV, while that of the bottom contact was fixed at 1.2 eV. We note once more that since P(VDF-TrFE) is an insulator, only injection into the semiconductor phase is considered. The top contact is the injecting contact. The current collecting bottom contact is grounded.

To calculate the current–voltage (J–V) characteristics, a field-dependent charge injection into the semiconductor is implemented via the Emtage/O'Dwyer model as described by van der Holst et al. [15] see Supporting Information. In this model, charge injection is assumed to take place by thermal excitation over an injection barrier that is lowered by the image potential. It should be stressed that only the details of the results presented below depend on the injection model, provided it is field dependent. All parameters are taken as reported in Ref. [11]. The electrical transport model is explained in detail in the Supporting Information.

Fig. 2 elucidates the lowering of the injection barrier by the ferroelectric polarization and the resulting current injection in the On-state. The schematic in Fig. 2a shows the polarization charges in the ferroelectric phase. The electric field lines (black arrows) run from positive to negative polarization charges. Importantly, near the top contact field lines also run from the positive image charges in the electrode to the negative polarization charges in the ferroelectric and similarly near the bottom contact. At the injecting top contact, it is the stray field of the positive image charges and the negative polarization charges, shown by the curved arrows, that causes the barrier lowering and locally enhances hole injection. Hence, the current, shown by the white arrows, is injected from the top contact into the semiconductor in close vicinity of the interface with the ferroelectric.

A zoom-in on the actual calculated potential and field lines in the injection region (dotted box in Fig. 2) is presented in Fig. 3. In the vicinity of the injecting top electrode ($y = 120$ nm) the y-component of the stray field indeed points away from the contact, in the same direction as the bias field and, therefore, enhances the hole injection. Using a polarization charge of $\sigma_p \sim 70\ \mathrm{mC/m^2}$ the stray field close to the interface between the phases is typically two orders of magnitude larger than the bias field in the semiconductor, given by $F = (V - V_{bi})/L$ with V_{bi} the built-in voltage. The corresponding image potential causes a substantial lowering of the hole injection barrier close to this interface. The contact becomes Ohmic and charges

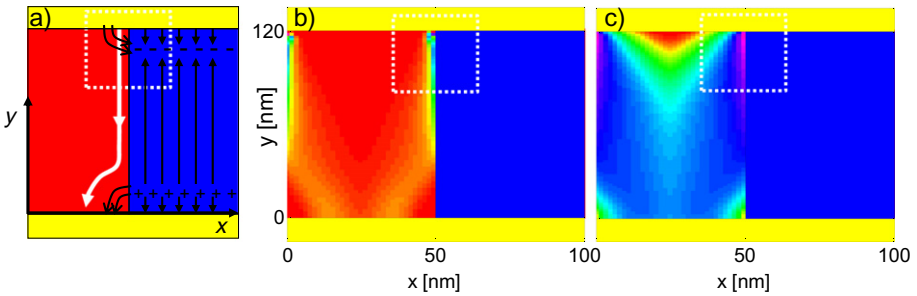

Fig. 2. (a) Schematic mechanism of injection barrier lowering and current injection. The ferroelectric, semiconductor and electrodes are indicated by blue, red and yellow planes, respectively. Black and white arrows indicate electric fields and current flow, respectively. + and − indicate polarization charges. See text for further explanation. (b) Current density, and (c) hole density (^{10}log-scale) of a ferroelectric diode in the on-state at 7 V. $_t$ = 0.7 eV, the top contact is at y = 120 nm. The dotted box indicates the region of highest interest of which Fig. 3 is a zoom-in. (For interpretation of the references to color in this figure legend, the reader is referred to the web version of this article.)

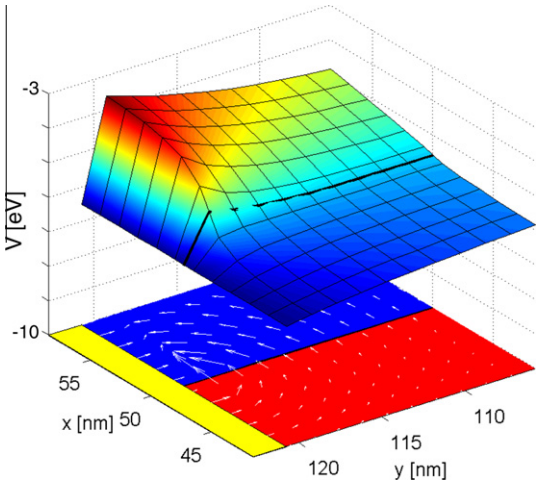

Fig. 3. Zoom-in near the injection point on the electrostatic potential (3D plane) and electric field lines (white arrows). The ferroelectric, semiconductor and electrodes are indicated by blue, red and yellow planes, respectively. For clarity the field arrows in the top two rows (around y = 120 nm) of the ferroelectric have been scaled by a factor 0.1. (For interpretation of the references to color in this figure legend, the reader is referred to the web version of this article.)

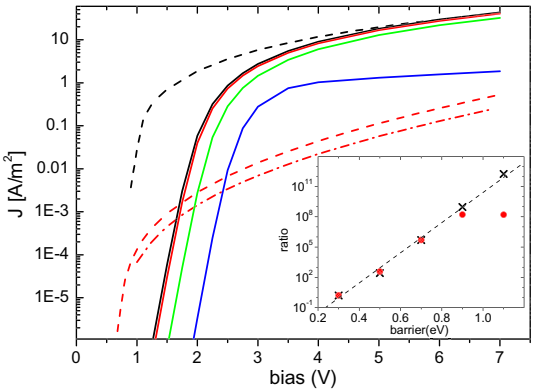

Fig. 4. Calculated current density–voltage characteristics for a 120 nm thick diode. Current densities J are averages over the contact area. Dashed lines are 1D calculations for a semiconductor-only diode with 0.1 eV (black) and 0.5 eV (red) injection barrier. The solid (On) and dash-dotted (Off) lines correspond to a 2D calculation for a ferroelectric diode with a slab width of 50 nm for both the semiconductor and the ferroelectric. The injection barrier of the top contact is varied from 0.3 eV (black), 0.5 eV (red), 0.7 eV (green) to 0.9 eV (blue). 'On' and 'Off' refer to a forward poled and unpoled ferroelectric, respectively. Inset: Calculated current ratios *vs.* top electrode injection barrier $_t$ at 4 V bias. Crosses: space-charge limited over injection limited current for a 1D semiconductor-only diode. Circles: On-current over Off-current for a 2D ferroelectric diode. The dashed line indicates a slope of 0.067 eV per decade. (For interpretation of the references to color in this figure legend, the reader is referred to the web version of this article.)

can be injected into the semiconductor phase. The lateral x-component of the stray field is directed towards the ferroelectric phase. Hence the injected holes (Fig. 2c) are accumulated at the phase boundary and consequently the current will be confined into narrow filaments (Fig. 2b). This spatial confinement causes space charge effects to limit the diode current in the On-state. In the lower half of the semiconductor phase the lateral x-component of the stray field becomes smaller and the current spreads over the whole semiconductor phase before it reaches the collecting contact at y = 0.

In the Off-state, *i.e.* positive ferroelectric polarization, electric field, charge and current density are distributed homogeneously throughout the semiconductor phase at the injecting electrode (not shown).

The fundamental results of the calculations are current–voltage (J–V) characteristics, of which a representative set is shown in Fig. 4. First we consider the semiconductor-only diode, without the ferroelectric phase. The dashed black line is calculated for a diode with a negligible top injection barrier φ_t of 0.1 eV. The small injection barrier gives rise to an Ohmic contact and hence to a space-charge limited current (SCLC) beyond an onset of ~1 V due to the built-in voltage. A larger top injection barrier φ_t of 0.5 eV causes the diode to become injection limited, as witnessed by the stronger bias dependence of the dashed red J–V curve.

In the next step, the ferroelectric slab is introduced in the same diode with an injection barrier φ_t of 0.5 eV. For an unpoled ferroelectric phase the injected current density is reduced by a factor 2 due to the reduced surface area of the semiconductor – the ferroelectric phase does not conduct current – but the functional shape of the J–V curve remains the same as in the semiconductor-only diode

(dash-dotted red line). When negative polarization charges are introduced in the ferroelectric slab, the injection limitation is relaxed. Above the effective built-in voltage the current becomes space charge limited. The solid green curves present calculated J–V characteristics for barriers φ_t between 0.3 eV and 0.9 eV. They show that the trend is persistent for barriers φ_t up to 0.9 eV, in good agreement with experiments [9,11].

The inset of Fig. 4 summarizes these findings by comparing the On/Off current ratio of the ferroelectric diode (red dots) to the ratio of the space charge limited current over the injection limited current of the semiconductor-only diodes (black crosses). Like in the experiments of Ref. [11], we find an almost exact overlap between the two ratios, both showing an exponential dependence upon injection barrier height. Two important conclusions can therefore be drawn. Firstly, it confirms that the injection limited diode in the Off-state is switched to a fully bulk (space charge) limited diode in the On-state. Secondly, it rationalizes the exponential dependence of the On/Off current ratio on barrier height that was reported in Ref. [11]. In an injection limited diode, the electric field $F = (V - V_{bi})/L$ is virtually constant, and the current density is given by Ohms' law as $J_{ILC} = qn_0\mu F$, with L, q and μ the layer thickness, elementary charge and mobility, respectively. In the Emtage/O'Dwyer injection model, like in virtually all injection models, the interfacial charge density n_0 depends exponentially on the (effective) injection barrier height φ_t. Hence, the injection limited Off-current depends exponentially on φ_t. The different slope found here as in compared to the one in Ref. [11], *viz.* 0.067 *vs.* 0.25 eV/decade and the lower maximum barrier height that can be turned Ohmic, *viz.* 0.9 *vs.* 1.3 eV, are due to an underestimation of the injection limited current by the employed model. The calculated SCLC currents however match very well to the measured ones.

In Fig. 4 the Off-currents refer to calculations with an unpoled instead of a reversely poled ferroelectric – the latter is normally used to define the on/off ratio. We deliberately used the unpoled current as a worst case scenario for the on/off current ratio. When the ferroelectric is reversely polarized, the stray field inhibits injection from the injection-limited contact even further. Therefore the reverse, or positively poled current is always lower than the unpoled current. The reason the unpoled current is more appropriate for comparison with experiment is the difference in cluster sizes between experiment and model. As shown above, the significant part of the stray field of the polarized ferroelectric penetrates at most a few tens of nm into the semiconductor. Hence, of the clusters in the experiments, which are several 100's of nm wide [12], the largest part experiences no significant polarization stray field and behaves like the device is in the unpoled state. In the calculations of Fig. 4a 50 nm wide cluster is used for computational reasons. For the on-state the lacking central part does not matter as the current runs at the interface. However, for the Off-state the lacking central part is crucial as the current near the interface is suppressed by the reversed stray field. For a 50 nm cluster this means that essentially the entire device current is suppressed. In order to compare with experiments the calculated unpoled current therefore has to be taken.

A major advantage of rectifying ferroelectric-driven organic resistive switches is that they can be integrated into crossbar memory arrays [1]. The rectification prevents cross-talk. A crossbar array combines a simple architecture with a high data density that scales as $4f^2$, with f the minimum feature size of the memory cell, typically the electrode width and spacing. The ultimate feature size corresponds to a single *semiconductor* domain enclosed by a thin ferroelectric shell. We therefore studied the scaling of the average current density with domain size. The average current density is defined as the total device current (that only runs in the semiconductor domain) divided by the total device area (that comprised both the semiconductor and ferroelectric domains and is kept constant). The dependence of the switching behavior on the semiconducting domain diameter is shown in Fig. 5a. We observe that for modest biases ($\leqslant$4 V) the average current density goes down for narrow (<50 nm) semiconductor clusters. A similar almost exponential behavior was experimentally observed [12]. This is a surprising result since the average current density for a constant area is plotted, and for all ferroelectric diodes shown the on-current remains concentrated in two narrow filaments at the edges of the semiconductor. The effect is due to the stray field in the bulk of the semiconductor domain. The polarization field between the positive and negative polarization charges in the ferroelectric also spreads out into the semiconductor, see Fig. 5b. In the discussion of Fig. 2 this bulk part of the stray field was ignored. As can be seen in Fig. 5b, it opposes the applied field (not shown) that points downward. Consequently, the closer the two sides of the ferroelectric material are together, *i.e.* the more narrow the semiconductor domain gets, the stronger the negative bulk field becomes. Therefore, at modest applied biases the current gets pinched off in narrow clusters. This current-blocking effect by the bulk stray field is also responsible for the current drop at low voltages in the (solid) 'On' curves of Fig. 4.

In Fig. 5c the qualitative argument above is quantified by a representative calculated potential. It can be seen that the potential in the semiconductor domain (x = 0–36 nm) is S-shaped at low bias, *i.e.* there is a negative (pointing towards the injecting contact) field behind the contact. This is indicated by the black arrow. The negative field blocks the charges after injection; hence they pile up, frustrating further injection and transport. At higher bias the S-shape is flattened out and the current becomes 'normal' SCLC again.

For the present parameters, Fig. 5a puts a lower limit of about 50 nm on the feature size that can experimentally be used in a crossbar array. We assume an idealized device layout in which ~50 nm (diameter) semiconductor domains are embedded in a ferroelectric matrix on a square lattice with a ~100 nm pitch. When properly aligned with word and bit lines a cross bar array like in Ref. [1] is formed. This device would be a rewritable memory with an information density of the order of 1 Gb/cm^2. In this estimate, we used the fact that for devices with narrow clusters the experimental Off-current is limited by leakage currents in the range 10^{-4}–10^{-6} A/m^2 at 2 V. The 1 Gb/cm^2 should thus be regarded as a conservative estimate of the upper limit that does not rely on suppression of already small Off-currents.

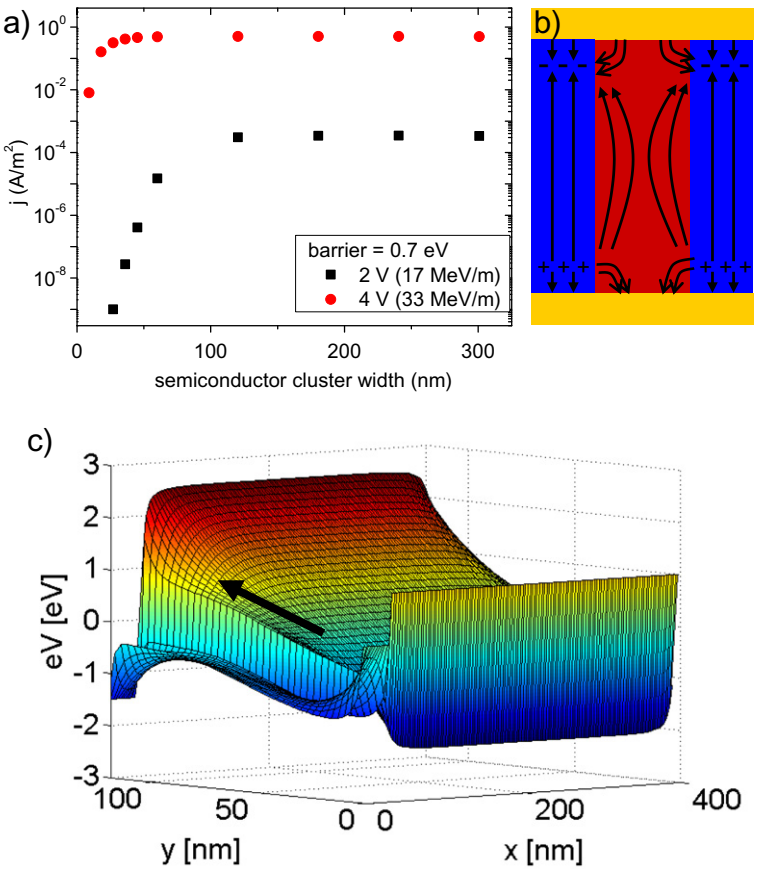

Fig. 5. (a) Calculated average current densities vs. width of the semiconductor cluster for various biases. Closed symbols denote on-currents. The device thickness is 120 nm, the total width (ferroelectric + semiconductor) is 400 nm. (b) Illustration explaining the reduction in on-current with decreasing cluster width. The ferroelectric, semiconductor and electrodes are indicated by blue, red and yellow planes, respectively. Black arrows indicate electric fields; + and − indicate polarization charges. See text for further explanation. (c) Calculated electrostatic potential for a ferroelectric diode with a 36 nm wide semiconductor domain at 2 V bias. The potential in the ferroelectric phase has been offset by 1 V for clarity. The black arrow indicates the direction and position of the negative electric field in the bulk of the semiconductor. (For interpretation of the references to color in this figure legend, the reader is referred to the web version of this article.)

In conclusion, we have elucidated and quantitatively explained the origin of the resistive switching in phase-separated ferroelectric-semiconductor blend diodes. The injection limited contact for charge injection into the semiconductor phase is turned into an Ohmic contact by the stray field of the polarized ferroelectric phase. The experimentally observed exponential scaling of the on/off current modulation ratio with injection barrier height has been quantitatively be reproduced. We estimate the optimum diameter of the semiconducting domains in a ferroelectric matrix as about 50 nm, and hereby predict the ultimate memory density that can be realized in the order of 1 Gb/cm^2. The model presented here is general and can also be used to investigate the significance of the stray field for the polarization of patterned inorganic ferroelectric microstructures [16].

Acknowledgment

We gratefully acknowledge financial support from EU project ONE-P, No. 212311.

Appendix A. Supplementary data

Supplementary data associated with this article can be found, in the online version, at doi:10.1016/j.orgel.2011.10.013.

References

[1] K. Asadi, M. Li, N. Stingelin, P.W.M. Blom, D.M. De Leeuw, Appl. Phys. Lett. 97 (2010) 193308.
[2] J.C. Scott, L.D. Bozano, Adv. Mater. 19 (2007) 1451.
[3] S. Möller, G. Perlov, W. Jackson, C. Taussig, S. Forrest, Nature 426 (2003) 166.
[4] B.C. de Brito, E.C.P. Smits, P.A. van Hal, T.C.T. Geuns, B. de Boer, C.J.M. Lasance, H.L. Gomes, D.M. de Leeuw, Adv. Mater. 20 (2008) 3750.
[5] E. Cantatore, T.C.T. Geuns, G.H. Gelinck, E. van Veenendaal, A.F.A. Gruijthuijsen, L. Schrijnemakers, S. Drews, D.M. de Leeuw, IEEE J. Solid-State Circ. 42 (2007) 84.
[6] R.C.G. Naber, K. Asadi, P.W. Blom, D.M. de Leeuw, B. de Boer, Adv. Mater. 22 (2010) 933.
[7] T. Furukawa, Phase Trans. 18 (1989) 143.
[8] R.C.G. Naber, C. Tanase, P.W.M. Blom, G.H. Gelinck, A.W. Marsman, F.J. Touwslager, S. Setayesh, D.M. de Leeuw, Nat. Mater. 4 (2005) 243.
[9] K. Asadi, D.M. de Leeuw, B. de Boer, P.W.M. Blom, Nat. Mater. 7 (2008) 547.

[10] R.C.G. Naber, J. Massolt, M. Spijkman, K. Asadi, P.W.M. Blom, D.M. De Leeuw, Appl. Phys. Lett. 90 (2007) 113509.
[11] K. Asadi, T.G. de Boer, P.W.M. Blom, D.M. De Leeuw, Adv. Funct. Mater. 19 (2009) 3173.
[12] K. Asadi, H.J. Wondergem, R. Saberi Moghaddam, C.R. McNeill, N. Stingelin, B. Noheda, P.W.M. Blom, D.M. de Leeuw, Adv. Funct. Mater. 21 (2011) 1887.
[13] C.R. McNeill, K. Asadi, B. Watts, P.W.M. Blom, D.M. de Leeuw, Small 6 (2010) 508.
[14] (a) K. Maturova, M. Kemerink, M.M. Wienk, D.S.H. Charrier, R.A.J. Janssen, Adv. Funct. Mater. 19 (2009) 1379;
(b) K. Maturova, S.S. van Bavel, M.M. Wienk, R.A.J. Janssen, M. Kemerink, Adv. Funct. Mater. 21 (2011) 261.
[15] J.J.M. van der Holst, M.A. Uijttewaal, R. Balasubramanian, R. Coehoorn, P.A. Bobbert, G.A. de Wijs, R.A. de Groot, Phys. Rev. B 79 (2009) 085203.
[16] F.D. Morrison, L. Ramsay, J.F. Scott, J. Phys-Condens. Mater. 15 (2003) L527.